Microsc. Microanal. Microstruct. **3** (1992) 501–516 DECEMBER **1992**, PAGE 501

Classification
Physics Abstracts
07.80 — 73.60B — 73.40

Microscale characterisation of epitaxial semiconducting homolayers.

II. Electron beam induced current

François Cleton([1]), Brigitte Sieber([1]) and Jean Luc Lorriaux([2])

([1]) Laboratoire de Structure et Propriétés de l'Etat Solide, Unité de Recherche Associée au CNRS n° 234, Bât. C6, Université des Sciences et Technologies de Lille, 59655 Villeneuve d'Ascq cedex, France
([2]) Université des Sciences et Technologies de Lille, 59655 Villeneuve d'Ascq cedex, France

(Received 9 July 1992, accepted 3 February 1993)

Résumé. — Nous avons modélisé la variation de l'efficacité de collecte du courant induit (EBIC), η_{CC}, avec la tension d'accélération des électrons incidents. La structure étudiée est identique à celle caractérisée dans la première partie de cet article. L'utilisation du courant induit permet de mesurer la longueur de diffusion des porteurs minoritaires ainsi que le dopage effectif de la première couche. La valeur des vitesses de recombinaison aux interfaces peut également être estimée par cette technique. A partir de l'étude expérimentale de deux échantillons fabriqués dans les mêmes conditions sur des substrats semi-isolants de provenance différente, nous avons mis en évidence une influence du substrat sur les valeurs de longueur de diffusion et de dopage effectif de la couche supérieure.

Abstract. — The dependence of the electron beam induced current (EBIC) collection efficiency η_{CC} on the electron beam voltage is modelled for the particular case of the GaAs homostructure studied in part I of this paper. The minority carrier diffusion length L_1 and the doping level N_{D_1} of the uppermost layer, as well as the value of the first and second interface recombination velocities V_1 and V_2 can be determined by this technique. The experiments, performed on two homostructures, grown in the same conditions, on semi-insulating substrates supplied by different manufacturers, indicate the influence of the substrate on the value of L_1 and N_{D_1}.

1. Introduction.

The high quality of optoelectronic materials, required for the development of submicron devices, can be assessed by means of various techniques. The use of an electron beam in a scanning electron microscope (SEM) to induce luminescence (CL) and/or a minority carrier current (EBIC), allows the characterisation of a semiconducting specimen in a volume of the order of few μm^3. The main

parameter accessible by these techniques is the minority carier diffusion length [1-10], and a local determination of the doping level is possible by EBIC [8-10]. In the case of multilayer structures, interface recombination velocities can also be determined [1, 11]. Nevertheless, for this kind of characterisation at a local scale, which rely on either luminescence intensity or EBIC collection efficiency curves, a model has to be established in order to fit the experimental curves.

In the first part of this paper [12], a model has been developed for homostructures which resemble field effect transistors. This model has been applied to the CL characterisation of silicon doped GaAs epitaxial layers grown by molecular beam epitaxy (MBE). A large number of parameters are involved in the formation of the CL signal, such as the minority carrier diffusion length, the optical absorption coefficient, the surface and interfaces recombination velocities and the thicknesses of both the uppermost and buffer layers.

A good way to decrease the number of parameters is to use the EBIC technique, instead of CL, where only minority carrier transport is involved.

Therefore, in order to characterise GaAs homostructures grown by MBE at 580°C, we have calculated, from the above mentioned model, the dependence of the EBIC collection efficiency on the accelerating beam voltage, i.e. on the electron penetration depth R. The structure used in our study consisted of a silicon doped ($n = 4 \times 10^{17}/\text{cm}^3$; thickness e_1) uppermost layer grown on an acceptor doped GaAs ($[N_a] \simeq 1 \times 10^{15}$ cm^{-3}; thickness e_2) buffer layer, the substrate being semi-insulating, chromium doped (001) oriented GaAs. The buffer layer can be considered as depleted from free carriers (Fig. 1). The EBIC current has been collected by a Schottky diode perpendicular to the electron beam. One specimen has been fabricated with a Wacker substrate, a second one with a Sumitomo substrate.

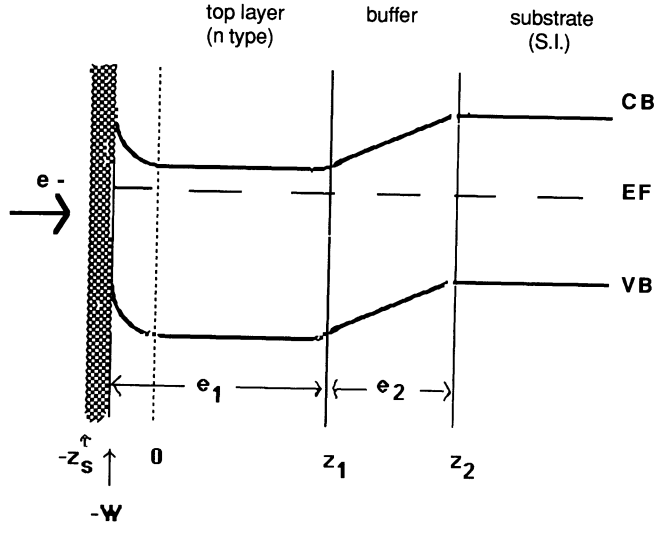

Fig. 1. — Schematic diagram of the GaAs homostructure. The Schottky diode is parallel to the surface and perpendicular to the electron beam. $Z_s = w + z_m$. See text for details.

The results obtained on both specimens display the influence of the substrate on the value of the diffusion length of the uppermost layer, and on the concentration of electrically active doping species.

2. Theoretical background.

We will recall the model previously developed for the specimen geometry investigated in this work (Fig. 1).

2.1 GENERAL. — The electron beam is perpendicular to the specimen surface and interfaces and parallel to the z axis; the origin is at the bottom of the space-charge-region (SCR) of width W.

The EBIC current collected by the diode is the sum of two currents: I_{SCR} generated in the SCR and I_{bulk} generated in the bulk region of the uppermost layer. Due to the cylindrical symmetry of the geometry, the EBIC currents in homogeneous regions are given by relations (1) and (2):

$$I_{SCR} = -e\, EC \int_{-W}^{0} g\,(z + z_s)\, dz \tag{1}$$

$$I_{bulk} = -e\, D_1 \left.\frac{d\,\Delta p_1(z)}{dz}\right|_{z=0} \tag{2}$$

I_{SCR} is easy to calculate when the one-dimensional generation function of electron-hole pairs $g\,(z + z_s)$ is known ($z_s = W + z_m$). We used the Gaussian analytical expression derived by Akamatsu *et al.* [13] for GaAs. The term EC in (1) is the collection efficiency in the SCR which can account for recombination in the SCR [10].

The calculation of the bulk EBIC current given by (2) requires the knowledge of the excess minority carrier density $\Delta p_1(z)$ in the uppermost layer. $\Delta p_1(z)$ obeys the one-dimensional steady-state diffusion equation which, under low injection conditions, in absence of electric field is:

$$D_1 \cdot \frac{d^2 \Delta p_1(z)}{dz^2} - \frac{\Delta p_1(z)}{\tau_1} = -\frac{g(z)}{D_1} \tag{3}$$

τ_1 and D_1 are the minority carrier lifetime and diffusion coefficient respectively. It was previously established that $\Delta p_1(z)$ has the following form [12]:

$$\Delta p_1(z) = A_1 \exp(z/L_1) + B_1 \exp(-z/L_1) + \frac{L_1}{2D_1} \int_0^{z_1} \exp\left(-\frac{|z - z'|}{L_1}\right) g\,(z' + z_s)\, dz' \tag{4}$$

At the bottom of the SCR ($z = 0$), the relation

$$\Delta p_1(z = 0) = 0 \tag{5}$$

expresses the collection of the minority carriers $\Delta p_1(z)$ by the electrical field of the SCR.

The minority carriers, of density $\Delta p_1(z)$, which reach, by diffusion, the first interface can be drifted by the electric field of the second layer where it is assumed that neither diffusion nor recombination occur [12].

The density $\Delta p_2(z)$ of minority carriers in the second layer is such that:

at the first interface $(z = z_1 = e_1 - W)$:

$$\mathbf{j}_2(z_1) - \mathbf{V}_{21}\Delta p_2(z_1) = \mathbf{j}_1(z_1) \tag{6}$$

$\mathbf{j}_1$ and $\mathbf{j}_2$ being the minority carrier current densities in layers 1 and 2 respectively; we have made in [12] the assumption that the recombination velocity of interface 1 is such that $V_{21} = V_{12}$.

at the second interface $(z = z_2 = e_1 + e_2 - W)$:

$$\mathbf{j}_2(z_2) - \mathbf{V}_{23}\Delta p_2(z_2) = \mathbf{j}_3(z_2) \tag{7}$$

$\mathbf{j}_2$ and $\mathbf{j}_3$ are the minority carrier current densities in layers 2 and 3 respectively; $\mathbf{j}_3$ is a diffusive current, and the density $\Delta p_3(z)$ has the same mathematical form as that of $\Delta p_1(z)$ [12]. The recombination velocity of interface 2 is such that $V_{23} = V_{32} = V_2$.

$\mathbf{j}_2(z)$ and $\mathbf{j}_3(z)$ are related by [12]:

$$j_2(z_2) = j_1(z_1) + GE \tag{8}$$

GE being the contribution of minority carriers created by the electron beam in the second layer:

$$GE = \int_{z_1}^{z_2} g(z + z_s)\,\mathrm{d}z \tag{9}$$

Equation (7) can therefore be written as [12]:

$$(\mu E - V_{23})\,\Delta p_3(z_2) = j_3(z_2) = -D_3 \frac{\mathrm{d}\,\Delta p_3(z)}{\mathrm{d}z}\bigg|_{z_2} \tag{10}$$

where μ is the minority carrier mobility and E the electric field in the second layer.

Equation (25) previously established in [12] for the cathodoluminescence intensity is still valid:

$$-D_1 \frac{\mathrm{d}\,\Delta p_1(z)}{\mathrm{d}z}\bigg|_{z_1} - (V_{12} + V_{23})\,\Delta p_1(z_1) + GE\left(1 - \frac{V_{23}}{\mu E}\right) = -D_3 \frac{\mathrm{d}\,\Delta p_3(z)}{\mathrm{d}z}\bigg|_{z_2} \tag{11}$$

The last relation needed to determine the values of the coefficients A_1, B_1, A_3 and B_3 is:

z infinite:

$$\Delta p_3(z) = 0 \tag{12}$$

The boundary conditions (5), (10), (11) and (12) lead to the following expressions of the coefficients:

$$A_3 = 0 \tag{13}$$

$$B_3 = \frac{\frac{IP_3}{2}\left(1 + (\mu E - V_{23}) \cdot \frac{L_3}{D_3} + 1\right)}{(D_3/L_3 + V_{23} - \mu E)} \exp\left(\frac{z_2}{L_3}\right) \tag{14}$$

with $$IP_3 = \int_{z_2}^{\infty} \exp\left(\frac{z_2 - z'}{L_3}\right) g(z')\,\mathrm{d}z' \tag{15}$$

$$A_1 = \frac{\beta\,(D_1/L_1 - (V_{12} + V_{23}))\exp(-z_1/L_1) - \alpha}{\Delta} \tag{16}$$

$$B_1 = \frac{\beta\,(D_1/L_1 + (V_{12} + V_{23}))\exp(z_1/L_1) + \alpha}{\Delta} \tag{17}$$

where

$$\begin{aligned}\Delta = {} & (D_1/L_1 - (V_{12} + V_{23}))\exp(-z_1/L_1) \\ & + (D_1/L_1 + (V_{12} + V_{23}))\exp(z_1/L_1)\end{aligned} \tag{18}$$

where

$$\beta = -\frac{L_1 \cdot IP_1}{2\,D_1} \tag{19}$$

$$\begin{aligned}\alpha = {} & \frac{IP_2}{2}\left(\frac{V_{12} + V_{23}}{D_1/L_1} - 1\right) - \frac{IP_3}{2} - GE\left(1 - \frac{V_{23}}{\mu E}\right) \\ & + \frac{D_3}{L_3} B_3 \exp\left(-\frac{z_2}{L_3}\right)\end{aligned} \tag{20}$$

with

$$IP_1 = \int_0^{z_1} \exp\left(\frac{-z'}{L_1}\right) g(z')\,\mathrm{d}z' \tag{21}$$

and

$$IP_2 = \int_{z_1}^{z_2} \exp\left(-\frac{z_1 - z'}{L_1}\right) g(z')\,\mathrm{d}z' \tag{22}$$

The final EBIC bulk current expression is:

$$I_{\text{bulk}} = -e\left(\frac{D_1}{L_1}(A_1 - B_1) + \frac{1}{2}\int_0^{z_1} \exp(-z/L_1)\, g(z' + z_s)\,\mathrm{d}z'\right) \tag{23}$$

2.2 RESULTS. — The EBIC collection efficiency η_{CC} is the ratio of experimental gain to the theoretical gain. In both the cases of bulk specimens and homostructures, η_{CC} passes through a maximum at a value E_{0m} of the beam accelerating voltage when E_0 increases. The value of E_{0m} depends on all the parameters involved in the EBIC process which are, in general: the metal thickness z_m of the diode, the doping level N_D determined from the SCR width W (Fig. 2), the collection efficiency EC in the SCR (Fig. 3) and the minority carrier diffusion length (Fig. 4). In the case of the homostructure investigated in this work, other parameters have also to be taken into consideration:

i) both the recombination velocities at the first and second interface, V_1 and V_2 respectively (Figs. 5 and 6). The sensitivity of the technique in the determination of the minority carrier diffusion length is dependent on V_1 and V_2 (Fig. 4): it is higher when V_1 and V_2 are smaller. As in the CL investigation [12], the interfaces recombination velocities have identical influence on the EBIC curves, and none of them cannot be really determined separately.

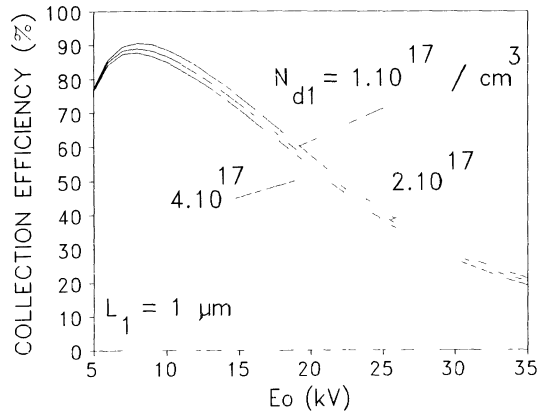

Fig. 2. — Influence of the doping level N_{d_1} on the theoretical EBIC collection efficiency curves as a function of the accelerating voltage E_0. The other parameters are: $e_1 = 1.5\ \mu$m; $e_2 = 0.8\ \mu$m; $z_m = 30$ nm; $L_1 = 1.0\ \mu$m; $L_3 = 1\ \mu$m; $V_1 > 10^3$ cm/s, $V_2 = 10^6$ cm/s; $EC = 1$. An increase in the doping level shifts the maximum of the curve towards low beam voltage as a result of the decrease of the SCR width.

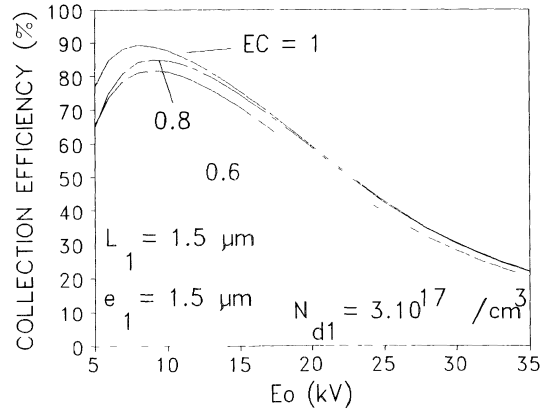

Fig. 3. — Influence of the SCR collection efficiency EC on the theoretical EBIC curves. The doping level of the uppermost layer is $3 \times 10^{17}/\text{cm}^3$. The other parameters are the same as in figure 2. When the value of EC decreases, E_{0m} increases.

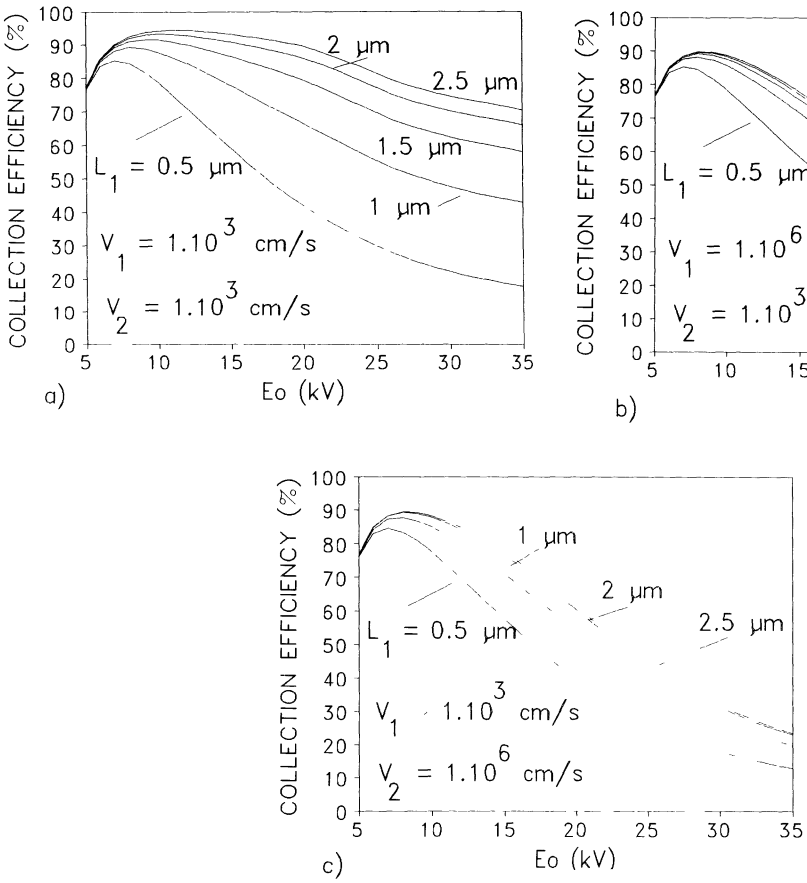

Fig. 4. — Influence of the diffusion length in the uppermost layer on the theoretical EBIC curves for different values of the first and second interface recombination rates. The other parameters are the same as in figure 2. a) $V_1 = 10^3$ cm/s; $V_2 = 10^3$ cm/s; b) $V_1 = 10^6$ cm/s; $V_2 = 10^3$ cm/s; c) $V_1 > 10^3$ cm/s; $V_2 = 10^6$ cm/s. An increase of the diffusion length leads to shift of the maximum towards higher beam voltages. This shift is a little larger when the recombination velocities of the interfaces are smaller.

ii) the thicknesses of the uppermost and second layers (Figs. 7 and 8)

iii) the value of the diffusion length L_3; this requires of course that the penetration depth of incident electrons is larger that $e_1 + e_2 + L_3$. In any case it will influence the curve at high beam voltages (Fig. 9).

From table I which shows the influence of all the parameters on the EBIC curves, we can see that the slope of the curve before the maximum is mainly dependent on L_1 (Fig. 4), N_{d_1} (Fig. 2), EC (Fig. 3) and e_1 (Fig. 7).

The slope of the curve after the maximum is mainly controlled by L_1 (Fig. 4) and, when L_1 is such that the ratio e_1/L_1 is smaller that 2, also by V_1 (Fig. 5a) and V_2 (Fig. 6a). In some cases, the thicknesses of the uppermost and buffer layer can also change drastically the slope of the curve (Figs. 7a, 8a).

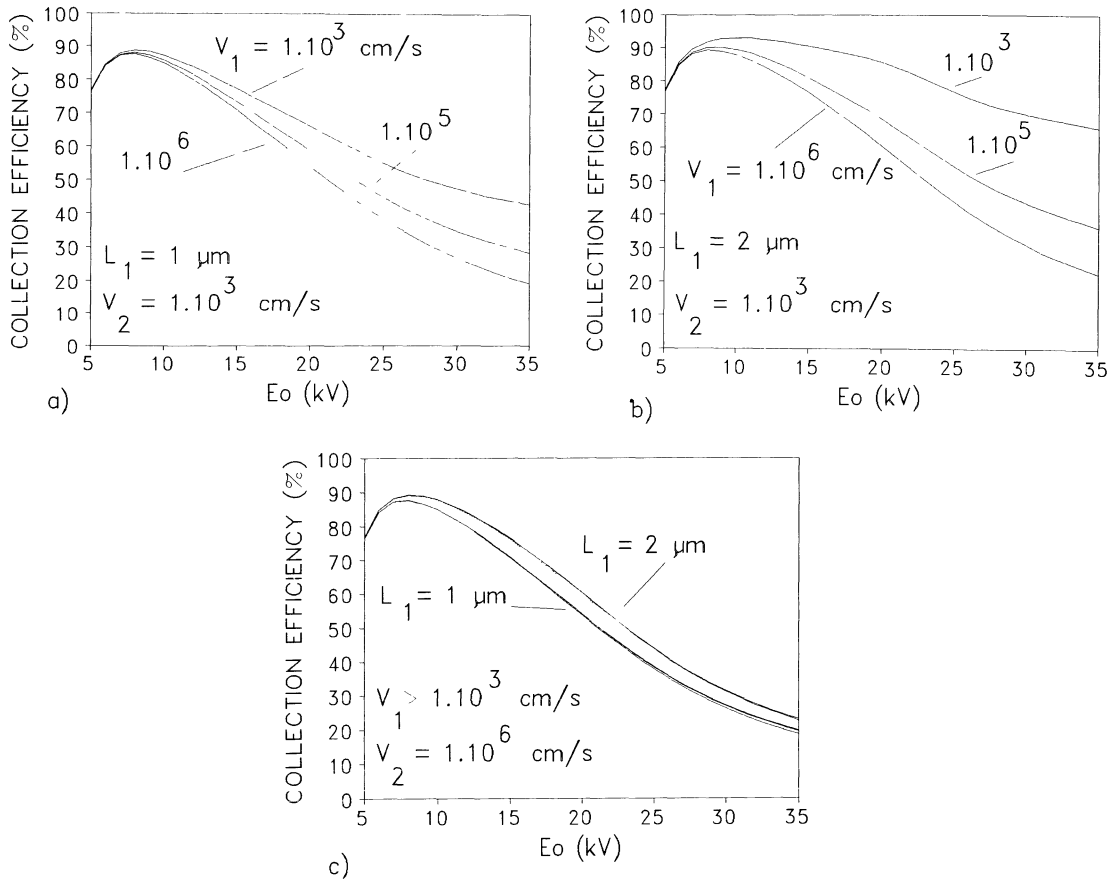

Fig. 5. — Influence of the first interface recombination velocity on the theoretical EBIC curves for different values of the diffusion length and second interface recombination rate. The other parameters are the same as in figure 2. a) $L_1 = 1$ µm; $V_2 = 10^3$ cm/s; b) $L_1 = 2$ µm; $V_2 = 10^3$ cm/s; c) $L_1 = 1$ µm and 2 µm; $V_2 = 10^6$ cm/s. An increase of V_1 leads to shift of the maximum towards lower beam voltages. This shift increases with the diffusion length in the uppermost layer (Fig. 5a, 5b). V_1 has no influence on the curves as soon as V_2 is as large as 10^6 cm/s, whatever is the diffusion length (Fig. 5c). The slope of the curve after the maximum decreases when V_1 increases.

3. Experiments

3.1 EXPERIMENTAL DETAILS. — The buffer layer of both samples was 0.8 µm thick. The uppermost layer of the specimen with a Wacker substrate was 2 µm thick, and it was 1.5 µm thick for the specimen with the Sumitomo substrate. Field effect transistors made on the uppermost layer provided the Schottky and the ohmic contacts needed for the EBIC experiments. The ohmic contacts were fabricated first by evaporation of the Au/Ge eutectic followed by sputtering of nickel and annealing at 465° C for 90 seconds in a nitrogen - oxygen (90/10) atmosphere. Then, the Schottky diodes were made by evaporating, in ultrahigh vacuum with an electron beam, titanium to a thickness of 45nm, through a mask of 50 x 80 µm^2 dimensions, and by heating the specimen up to 280° C for 20 minutes in a nitrogen-oxygen (90/10) atmosphere. The effect of diode annealing was investigated on the homostructure grown on the Sumitomo substrate. Such a large grid was used

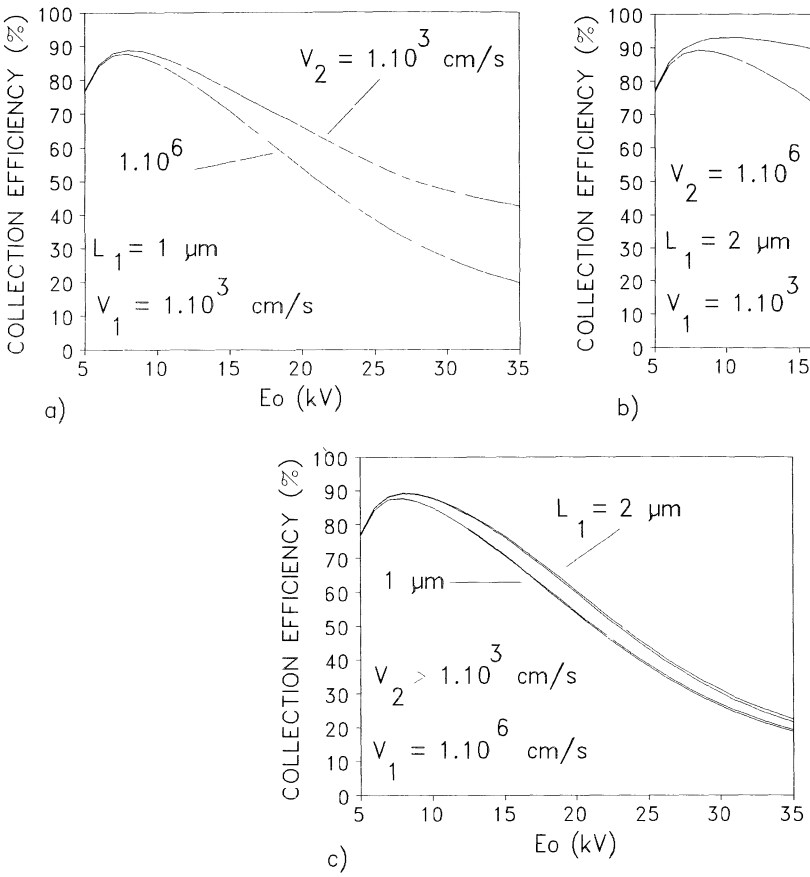

Fig. 6. — Influence of the first interface recombination velocity on the theoretical EBIC curves for different values of the diffusion length and second interface recombination rate. The other parameters are the same as in figure 2. a) $L_1 = 1$ µm; $V_1 = 10^3$ cm/s; b) $L_1 = 2$ µm; $V_1 = 10^3$ cm/s; c) $L_1 = 1$ µm and 2 µm; $V_1 = 10^6$ cm/s. The influence of V_2 on EBIC curves is similar to that of V_1 : see figure 5 captions for details.

because the resolution of the EBIC technique is of the order of 1 µm. The FETs were mounted in a Stereoscan 250 MK3 Cambridge scanning electron microscope. The EBIC currents were detected by a home-made amplifier located on the chamber of the SEM. The electron beam current, measured by a Faraday cup with a Keithley 616 ammeter, was ajusted for each accelerating voltage in order to achieve a constant beam power of 1×10^{-7} W.

3.2 RESULTS. — An increase of the electron beam voltage E_0 corresponds to an in-depth scan of the material since it leads to an increase of the electron penetration r_1 via the relation [14]:

$$r_1(\mu\text{m}) = \frac{4.57\, E_0^{1.75}(\text{kV})}{100\, \rho} \tag{24}$$

where ρ is the material density.

Before undertaking any quantitative measurements, EBIC pictures were taken as a function of E_0 with the aim of locating any inhomogeneity in the material.

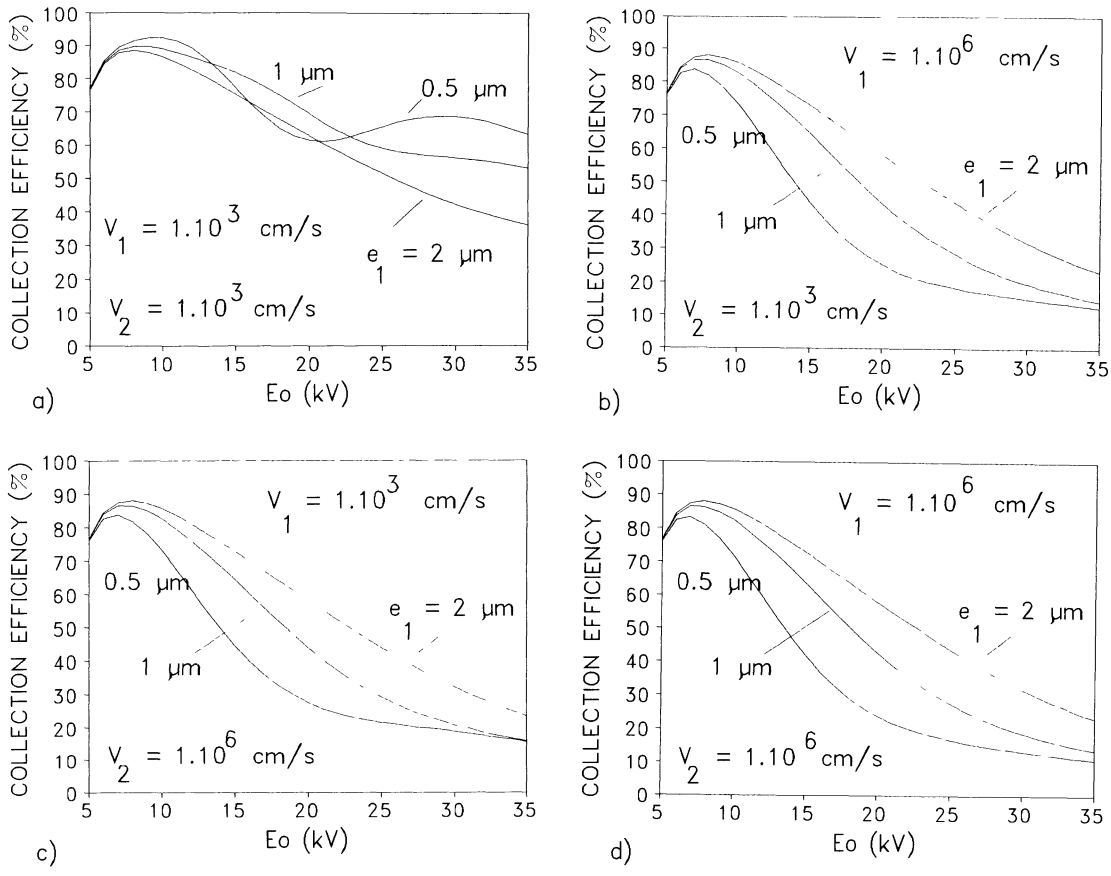

Fig. 7. — Influence of the thickness of the uppermost layer on the theoretical EBIC curves for $L_1 = L_3 = 1\ \mu m$ and for different values of the first and second interface recombination rates. The other parameters are the same as in figure 2. a) $V_1 = V_2 = 10^3$ cm/s; b) $V_1 = 10^6$ cm/s; $V_2 = 10^3$ cm/s; c) $V_1 = 10^3$ cm/s; $V_2 = 10^6$ cm/s; d) $V_1 = V_2 = 10^6$ cm/s. When V_1 and V_2 are equal to 10^3 cm/s, a second maximum can appear in the EBIC curve when e_1 is as small as 0.5 μm; in that case only, the EBIC collection efficiency at high beam voltages is higher than for thicker uppermost layers (Fig. 7a).

3.2.1 *Wacker SI substrate* — At low accelerating voltage, for instance 7 kV in figure 10 for $r_1 = 0.2\ \mu m$, the information displayed on the EBIC image of a specimen grown on the Wacker substrate exhibits fine inhomogeneities ("orange peel"). Although the electron beam reaches the diffusive region and that the majority of the electron-hole pairs are created within the SCR ($N_{D_1} = 4.\ 10^{17}\ cm^{-3} : W = 0.05\ \mu m$; $N_{D_1} = 2 \times 10^{17}\ cm^{-3} : W = 0.07\ \mu m$), the inhomogeneities were more probably related to technological problems, for instance a shrinkage of the metal during diode annealing. This could be the consequence of a bad state of the free surface prior to metal deposition. The dark spots visible in figure 10, whose size increases with E_0, have not been identified yet. At E_0 values higher than 12 kV, larger inhomogeneities are detected instead of the "orange peel" (Fig. 10b). They can be classified in dark and bright areas which correspond respectively to smaller and higher EBIC currents. Since the penetration depth of a 12 kV electron beam is 0.67 μm, it can be stated with confidence that the observed modulations are representative of the structure (uppermost layer + interfaces) and not related to technological problems.

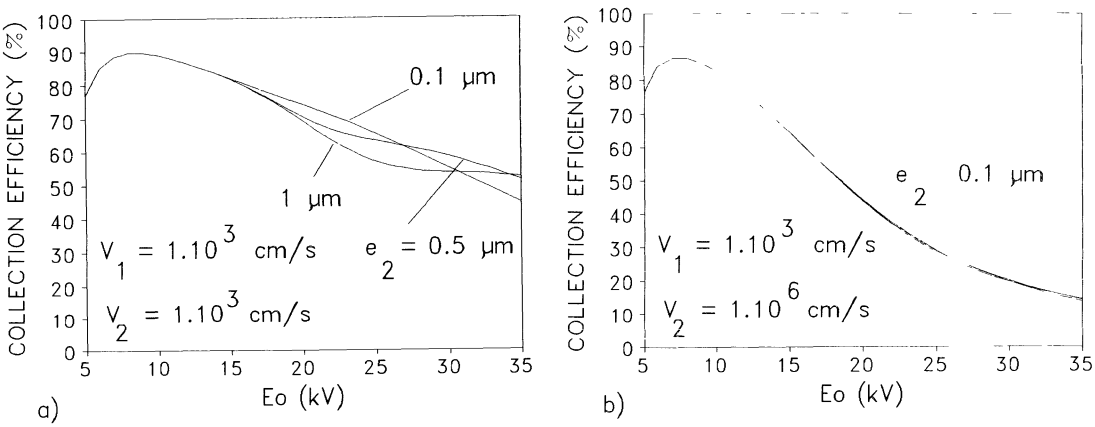

Fig. 8. — Influence of the thickness of the buffer layer on the theoretical EBIC curves for $L_1 = L_3 = 1$ μm and for different values of the first and second interface recombination rates. The other parameters are the same as in figure 2. a) $V_1 = V_2 = 10^3$ cm/s; b) $V_1 = 10^6$ cm/s and $V_2 = 10^3$ cm/s or $V_1 = 10^3$ cm/s; $V_2 = 10^6$ cm/s or $V_1 = V_2 = 10^6$ cm/s. When V_1 and V_2 are equal to 10^3 cm/s, a second maximum can appear in the EBIC curve when e_2 is as small as 0.5 μm; in that case only , the EBIC collection efficiency at is higher than for thicker buffer layers for few high beam voltage values (Fig. 8a). When one of the interface recombination rates is equal to 10^6 cm/s, e_2 has no influence on the EBIC curve (Fig. 8b).

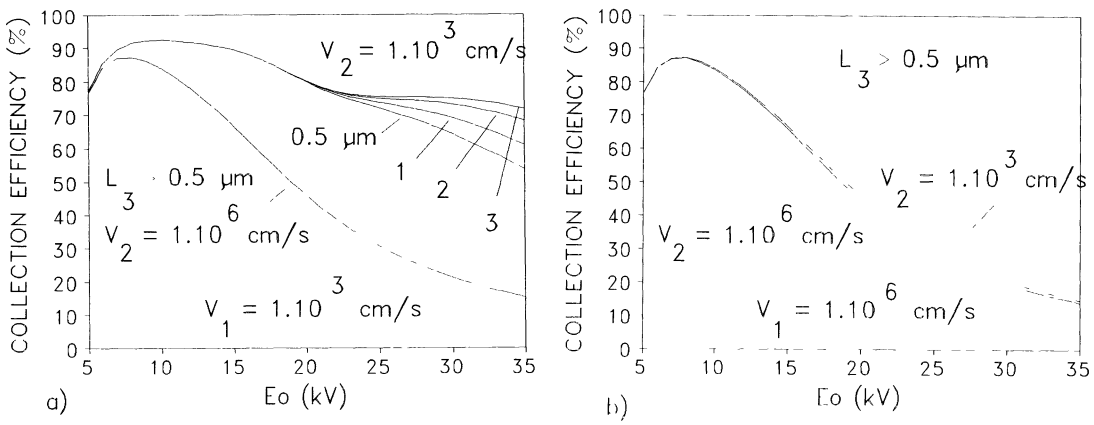

Fig. 9. — Influence of the diffusion in the substrate L_3 on the theoretical EBIC curves for $L_1 = 1$ μm and for different values of the first and second interface recombination rates. The other parameters are the same as in figure 2. a) $V_1 = 10^3$ cm/s; $V_2 = 10^3$ cm/s and 10^6 cm/s. b) $V_1 = 10^6$ cm/s; $V_2 = 10^3$ and 10^6 cm/s. In case a) a second maximum can occur in the EBIC curve at high beam voltages when V_2 is as small as 10^3 cm/s. For other combinations of V_1 and V_2, the diffusion length L_3 has no influence on the EBIC curves.

To identify exactly their origin, and in order not to get average values, the collection efficiency EBIC curves presented hereafter have been made in areas larger than the generation volume of electron-hole pairs (Fig. 10). The results of the fits (Fig. 11) reveal a slight difference in the diffusion length L_1 between the dark and bright areas (1 μm and 1.1 μm, see Tab. I). The doping level, which is estimated from the value of the SCR, is only half of that expected from the growth

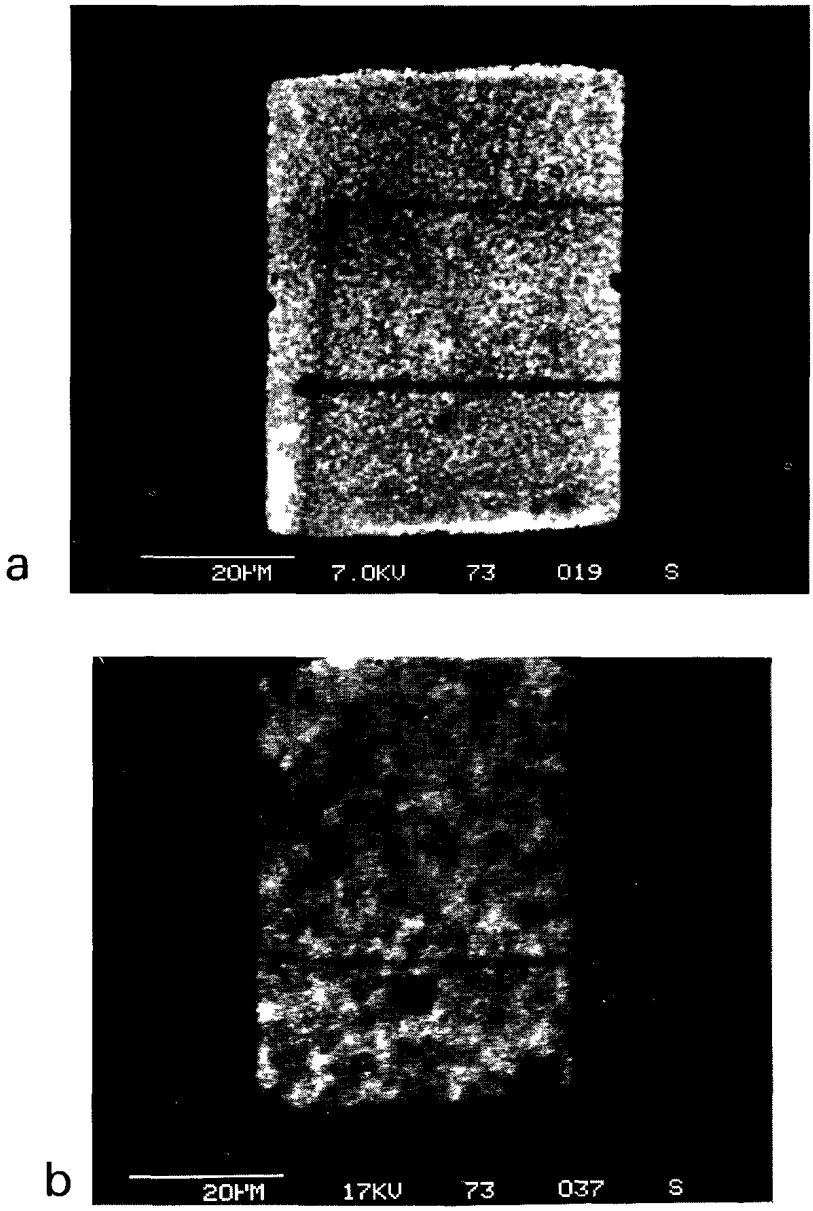

Fig. 10. — EBIC micrographs of the Wacker structure. a) At $E_0 = 7$ kV is evidenced on "orange peel" aspect of the metallization related to technological problems The two horizontal dark lines have been produced by the electron beam of the microscope b) At $E_0 = 12$ kV, the electron beam penetrates deeply within the uppermost layer Inhomogeneities are evidenced in the form of dark and bright areas.

conditions (2×10^{17} cm^{-3} instead of 4×10^{17} cm^{-3}) This is likely to mean that there is quite a high concentration of deep levels in the uppermost layer to compensate half of the silicon atoms introduced during growth. The very low SCR collection efficiency (about 15 %) supports this conclusion. The value of the first and second interface recombination velocities V_1 and V_2 were found to be close to 1×10^3 cm/s

Table I.

parameters influence	L_1	L_3	N_{D_1}	V_1	V_2	EC	e_1	$e_1 - e_2$
presence of a maximum	no	yes(*)	yes	no	no	no	yes(*)	yes(*)
position of the maximum	strong (→)	no	strong (←)	yes (←)	yes (←)	yes (←)	yes (→)	no
lst part of the curve	yes	no	yes	no	no	strong	yes	no
2nd part of the curve	strong	yes	no	strong	strong	no	yes(**)	yes(**)

(*) a second maximum can occur in the case $V_1 = V_2 = 10^3$ cm/s
(**) if $V_1 = V_2 = 10^3$ cm/s

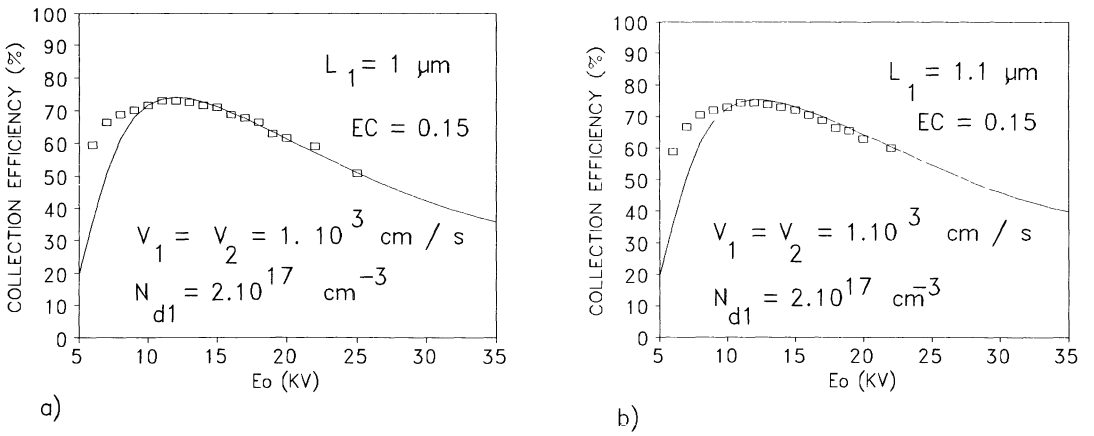

Fig. 11. — Fits of the EBIC curves for the Wacker sample. The EBIC inhomogeneities seen in figure 10 are the result of variation of the diffusion length (see tab. II). $e_1 = 2$ µm; $e_2 = 0.8$ µm; $z_m = 30$ nm; $V_1 = V_2 = 10^3$ cm/s. a) dark areas; b) bright areas.

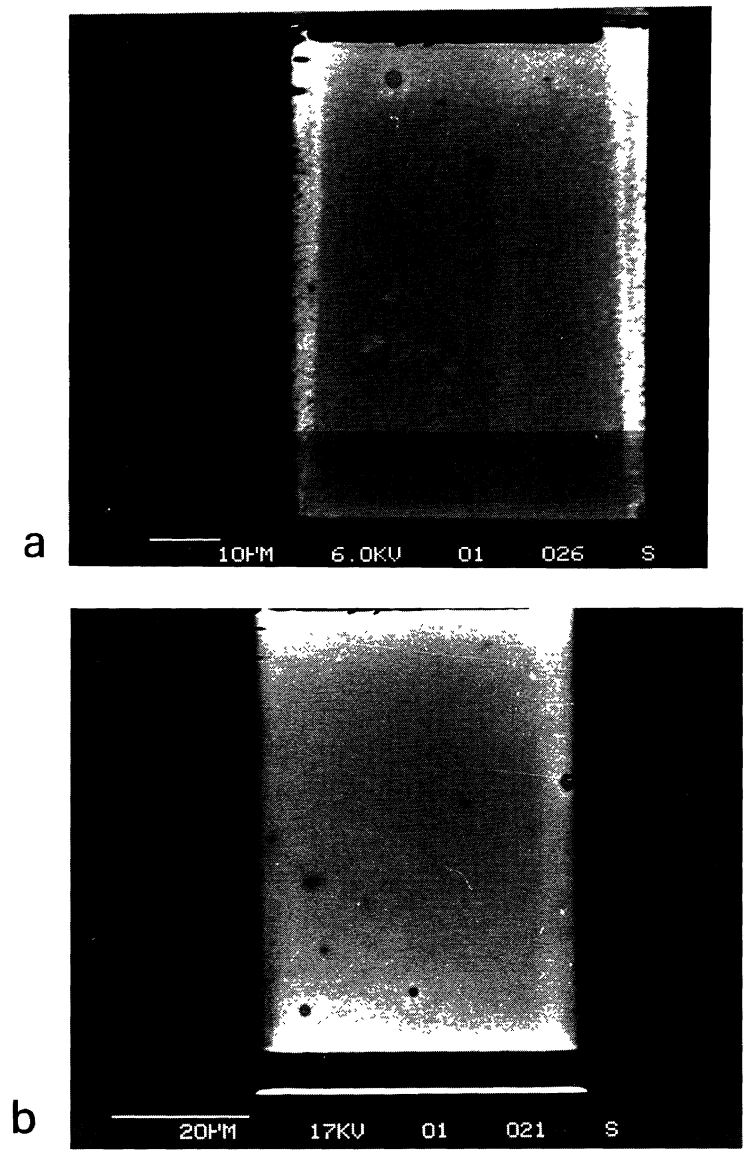

Fig. 12. — EBIC micrographs of the Sumitomo structure. a) $E_0 = 6$ kV; b) $E_0 = 11$ kV. The uppermost GaAs layer is more homogeneous and the only visible defects are dust particles on the metal.

The very beginning of both experimental curves is not fitted with our theoretical curves. This discrepancy could be related to generation centers at the metal-semiconductor interface of the Schottky diode. Such centers could result from the preparation of the diode. Further experiments have to be undertaken to ascertain this assumption and to identify the nature of the centers. Such information could be given by EBIC measurements as a function of reverse applied biais in order to increase the sensitivity of the SCR in-depth scan. The EBIC results could be correlated with deep level transient spectroscopy experiments (DLTS) in order to derive the energy level of the centers. The EBIC curves will have to be fitted by theoretical curves where the EBIC current in

the SCR will take account of both kind of centers, within the SCR and at the metal-semiconductor interface.

3.2.2 *Sumitomo SI substrate* — When imaged by EBIC at low and higher beam voltages the sample grown on the Sumitomo substrate (Fig. 12) appeared much more homogeneous than that grown on the Wacker substrate. Figure 13 shows the EBIC efficiency curves for the Sumitomo sample. The diffusion length is about 50% larger than in the Wacker sample, and the SCR collection efficiency is the double. Furthermore, the estimation of the doping level is closer to that expected from the growth conditions than that found in the Wacker sample (Tab. II). These three results are consistent, since the diffusion length is controlled by deeps levels at room temperature [10]. They indicate a higher quality of the uppermost GaAs layer of the Sumitomo homostructure, compared with that of the wacker substrate. It probably results from a smaller density of deep levels, or from their absence. More experiments, such as DLTS for instance, would provide an identification of these levels. Nevertheless, from our EBIC results, it can be ascertained that they arose from the substrate.

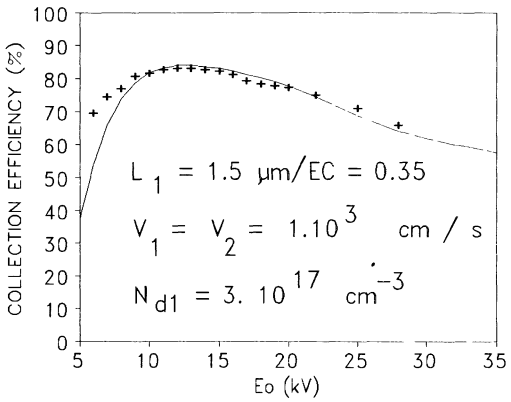

Fig. 13. — Fits of the EBIC curves for the Sumitomo sample. $e_1 = 1.5\ \mu m$; $e_2 = 0.8\ \mu m$.

Table II.

	Sumitomo	Wacker	
		Dark area	Bright area
L_1	1.5 μm	1.0 μm	1.1 μm
EC	0.35	0.15	0.15
N_{D_1}	$3 \times 10^{17}/cm^3$	$2 \times 10^{17}/cm^3$	
V_1, V_2	10^3 cm/s	10^3 cm/s	

The first and second interface recombination velocities have been found as low as 10^3 cm/s in both structures (Tab. II). This indicates that, no recombination levels being present at the interfaces, these homostructures are very suitable for making devices such as field effect transistors for instance.

4. Conclusion

We performed an EBIC investigation of the electrical properties of silicon doped GaAs homostructures grown on semi-insulating chromium doped substrates provided by two manufacturers. The MBE growth conditions were identical for both samples. We could evidence easily and rapidly marked differences between both samples in the electrical characteristics of their uppermost layer; the smaller values of the diffusion length, of the doping level and of the SCR collection efficiency in one sample are likely to be a consequence of a higher concentration of deep levels. These levels could originate from the substrate, or could be introduced, in one of the growth experiments, in a greater quantity. The first and second interface recombination velocities V_1 and V_2 were determined in both samples and were found as low as 10^3 cm/s. More EBIC experiments and more elaborate calculations are in progress to investigate more precisely the SCR and the metal-semiconductor interface.

Acknowledgements.

The authors thank Dr Y. Druelle (IEMN) for providing the MBE specimens. M. François is also acknowledged for the fabrication of the Fets.

References

[1] for a review, see for example KITTLER M. and SEIFERT W., Beam Injection Assessment of Defects in Semiconductors, Meudon-Bellevue, 1988, *Rev. Phys. Appl.* **C6** (1989) 31.
[2] HERGERT W., RECK P., PASEMANN L., SCHREIBER J., *Phys. Stat. Sol. (a)* **101** (1987) 611.
[3] HERGERT W., HILDEBRANDT S. and PASEMANN L., *Phys. Stat. Sol. (a)* **102** (1987) 819.
[4] HILDEBRANDT S., SCHREIBER J., HERGERT W. and PETROV V.I., *Phys. Stat. Sol. (a)* **110** (1988) 283.
[5] KOCH F., HERGERT W., OELGART G. and PUHLMANN N., *Phys. Stat. Sol. (a)* **109** (1988) 261.
[6] ACHOUR S., *Phil. Mag. Lett.* **59** (1989) 205.
[7] PUHLMANN N. and OELGART G., *Phys. Stat. Sol. (a)* **122** (1990) 705.
[8] WU C.J. and WITTRY D.B., *J. Appl. Phys.* **49** (1978) 2827.
[9] FRIGERI C., Microscopy of Semiconducting Materials, Oxford 1987, *Inst. Phys. Conf. Ser.* **87** (1987) 745.
[10] SIEBER B. and CARTON P., *Phys. Stat. Sol. (a)* **127** (1991) 423.
[11] KONNIKOV S.G. *et al., Soviet Phys. Semicond.* **20** (1986) 661.
[12] DE MEERSCHMAN Ch., SIEBER B., FARVACQUE J.L. and DRUELLE Y. , part I of this paper.
[13] AKAMATSU B., HENOC P. and MARTINS R.B., *J. Microsc. Spectrosc. Electron* **14** (1989) 12.
[14] GRUEN A.E., *Z. Naturforsh.* **12A** (1957) 89.